Understanding of the Finite Size Effects on Lattice Vibrations and Electronic Transitions of Nano α-Fe_2O_3

Li Lu,[†,‡] Liping Li,[†] Xiaojing Wang,[‡] and Guangshe Li*[,†]

Key Lab of Structural Chemistry, Fujian Institute of Research on the Structure of Matter, Chinese Academy of Science, Fuzhou 350002, People's Republic of China, and School of Chemistry and Chemical Engineering, Inner Mongolia University, Hohhot 010021, People's Republic of China

Received: May 26, 2005; In Final Form: July 23, 2005

α-Fe_2O_3 nanocrystals with controlled diameters ranging from 10 to 63 nm were successfully prepared. The finite size effects in α-Fe_2O_3 nanocrystals were probed by X-ray diffraction, infrared spectroscopy, thermogravimetric analysis, UV−visible spectrum, and magnetization measurements. With a size reduction, α-Fe_2O_3 nanocrystals showed a lattice expansion and an enlarged axial ratio of *c*/*a* that is in apparent contradiction to the previous conjecture of high lattice symmetry for α-Fe_2O_3 nanocrystals at small sizes. The surface terminations of α-Fe_2O_3 nanocrystals were found to be highly hydrated with a size dependence that surprisingly follows the surface hydration chemistry of anatase TiO_2 nanocrystals reported recently by us. The lattice vibrations, electronic transitions, and magnetic properties of α-Fe_2O_3 nanocrystals were significantly modified by surface hydration and lattice expansion. The finite size effects that occurred in α-Fe_2O_3 nanocrystals at small sizes were first found to give a red shift in frequencies of perpendicular mode at 540 cm^{-1}, a blue shift in the electronic transition of double exciton process in visible region, and a significant decrease in the coercive force.

Introduction

Iron oxides have received much attention owing to their potential applications in high-density recording media, pigments, catalysts, and gas sensors, as well as in geochemistry and mineralogical processes. The structural stability and electronic spectra of iron oxides are directly relevant to the current problems in these applications. It is well-known that the electronic transitions and optical spectra of iron oxides can provide information on the mechanisms of super-exchange interactions for abnormal magnetic behaviors,[1,2] chemical absorptions, the dynamics of charge carriers at liquid-semiconductor interfaces, and even the sunlight-induced photochemical reactions between colloidal iron oxides and organic materials in natural water.[3] Although nanoscale iron oxides are among the most useful materials for mentioned-above technological applications, their vibrational properties and electronic spectra are poorly known or understood. This is probably due to (1) the controversies[4−7] that remain unsolved about the structural stabilities and bonding nature of α-Fe_2O_3 within the nanoscale regime, and (2) the complex spectra[8] of Fe_2O_3 that not only consist of electronic transitions located to the $Fe−O_6$ coordination site (e.g., Fe^{3+} ligand field and $O^{2-}−Fe^{3+}$ charge-transfer transitions), but also exhibit phenomena resulting from the interactions between adjacent Fe^{3+} ions.

Ayyub et al.[4] studied the size effects on the structural stabilities of α-Fe_2O_3 and concluded that nanometer sized α-Fe_2O_3 is unstable below 30 nm and transforms into γ-Fe_2O_3. However, large amounts of literature[5−7] have shown that α-Fe_2O_3 can be stabilized to several nanometers. In certain reaction systems,[7] α-Fe_2O_3 nanocrystals, when comparing with γ-Fe_2O_3, appear to be more stable by their preferential formation at small sizes. Though still not being verified experimentally, the lattice of α-Fe_2O_3 has been presumed to become highly symmetric with a size reduction to nanoscale regime,[9] since the lattice expansion at nanoscale may have an inverse effect of an external pressure under which the inter-ionic bonds may lose their directional character for higher symmetry and increased covalency. This assumption is questionable since, with increasing the external pressures, the axial ratio, c/a, of bulk α-Fe_2O_3 has already been found to decrease,[10] while the lattice symmetry is much improved simultaneously, which are all inconsistent with what is expected from the assumption.

As common with many nanocrystals, structural properties and electronic transitions are significantly influenced by finite size effects. Extensive studies have been performed on the infrared optical properties of α-Fe_2O_3,[11,12] but the particles reported are too large (i.e., at micron level) to give pronounced quantum size effects in lattice vibrations and electronic transitions for band modifications. In the view of the fact that the interactions between 3d electrons of the metals and the oxygen nucleus determine the covalency of the solids and that the lattice variations and electronic transitions of solids are closely dependent on the structural characteristics, in this work, we explore the finite size effects on the structural properties and electronic transitions in α-Fe_2O_3 nanocrystals. We found that with a size reduction, the surfaces of all α-Fe_2O_3 nanoparticles became highly hydrated, while the lattice volume of α-Fe_2O_3 nanoparticles increased which is accompanied by a lowered lattice symmetry and an enhanced ionicity. The finite size effects were indicated by a red shift in the frequencies of perpendicular mode at 540 cm^{-1} in infrared region, a blue shift in the transition for double exciton process in visible region, and a significant decrease in coercive force.

* Corresponding author. E-mail: guangshe@fjirsm.ac.cn. Tel: +86-591-83702122. Fax: +86-591-83714946.
† Fujian Institute of Research on the Structure of Matter.
‡ Inner Mongolia University.

10.1021/jp052780+ CCC: $30.25
Published on Web 08/23/2005

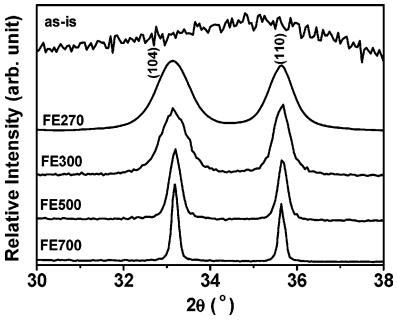

Figure 1. Enlarged XRD patterns for (104) and (110) peaks of α-Fe_2O_3 samples.

Experimental Section

Chemicals of $Fe(NO_3)_3 \cdot 9H_2O$ (>98.5% pure) and $NH_3 \cdot H_2O$ (25 wt %) were used as the starting material. $NH_3 \cdot H_2O$ solution was slowly added to 100 mL of 0.5 M $Fe(NO_3)_3$ solution while stirring to get a brown suspension solution at pH 8. After aging the suspension solution at room temperature in air for 8 h, a precipitate was formed, which was then washed fully with distilled water and dried in an oven at 60 °C for 4 h. The as-prepared powder was annealed at given temperatures of 270, 300, 400, 500, 560, 600, and 700 °C for 2 h in air. The samples thus obtained were named as FE270, FE300, FE400, and so on.

The structures of the samples were characterized by X-ray diffraction (XRD) on Rigaku DMAX2500 X-ray diffractometer using a copper target. The average grain sizes, D, were measured from the most intense XRD peak (104) using the Scherrer formula, $D = 0.9\lambda/(\beta \cos \theta)$, where λ is the X-ray wavelength employed, θ is the diffraction angle of the most intense peak (104), and β is defined as the halfwidth after subtracting the instrumental broadening. The lattice parameters were calculated using Retica Rietveld program with peak positions that are calibrated by internal standard of silica (99.99% pure).

The particle sizes and morphologies of the samples were determined using transmission electron microscopy (TEM) on a JEM-2010 apparatus with an acceleration voltage of 200 kV. The chemical compositions were examined with an energy-dispersive X-ray spectrometer (EDX) analysis. The infrared optical properties were measured on a Perkin-Elmer IR spectrophotometer using a KBr pellet technique. Water content of the samples was determined using thermogravimetric analysis (TGA) at a heating rate of 10 °C/min from room temperature to 1000 °C in a N_2 atmosphere at a flux of 40 mL/min and under ambient atmospheric pressure.

The optical diffuse reflectance spectra of α-Fe_2O_3 nanocrystals were obtained using Lambda 35 UV/VIS Spectrometer at room temperature in a wavelength region between 400 and 1100 nm. $BaSO_4$ was used as a reference material. The reflectance spectra were converted to the Kubelka−Munk remission function defined by $F(R) = (1 - R)^2/2R$, where R is the reflectance. The minima in the second-derivative curves of the Kubelka−Munk function were taken as the position for the absorption bands. The magnetization of the samples was measured at room temperature with an applied field of 85 KOe using a Quantum Design PPMS-7 magnetometer.

Results

Figure 1 shows the enlarged XRD patterns over a scan interval from $2\theta = 30-38°$ for the samples prepared at different temperatures. From Figure 1, it is seen that the as-prepared powder was amorphous and did not show any diffraction peaks.

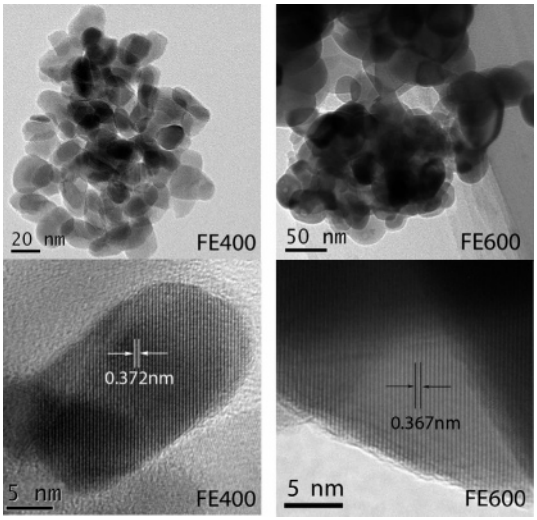

Figure 2. TEM images (top) and HRTEM photos (bottom) of samples FE400 and FE600.

When the as-prepared powder was heated at a temperature of 270 °C, as illustrated in Figure 1, a crystalline phase was formed in FE270, while no dispersed peaks associated with amorphous phases were observed. All diffraction peaks in Figure 1 matched the standard data for α-Fe_2O_3 (JCPDS 33-664) except for a systematic data shift. A careful examination of the XRD data for FE270 did not show any traces of other phases such as β-, γ-, δ- Fe_2O_3, or iron oxide hydroxides. EDX analysis showed the presence of Fe and O only. All these results demonstrated that sample FE270 had a high phase purity of the corundum structure. Further, sample FE270 showed relatively broad diffraction peaks, which indicated the fine nature of the particles. The average particle size measured from peak broadening of (104) line using Scherrer formula was about 10 nm for FE270. With increasing treatment temperature, a pronounced grain growth occurred as is confirmed by XRD data analysis (Figure 1) and TEM observations (Figure 2). For FE300, FE500, and FE700, the average particle sizes calculated by XRD data are 13, 33, and 63 nm, respectively. TEM photos for FE400 and FE600 are shown at the top of Figure 2, in which high-temperature treatment are indicated to give large sizes, and all particles are seen uniformly distributed in sheetlike shape except for a slight aggregation. The corresponding high resolution transmission electron microscopy (HRTEM) photos (bottom of Figure 2) clearly show that all particles were fully crystallized into tiny single crystals with high crystallinity, while the amorphous phases or short-range disordering distribution are barely observed at sample surfaces. These TEM observations are consistent with our XRD analysis. The spacings between adjacent lattice fringes are 0.372 nm for FE400 and 0.367 nm for FE600, respectively, which are much closer to the d-spacings of 0.369 and 0.367 nm for the (012) plane as calculated by XRD. It is also seen that the spacings of the lattice fringes became larger at lowered treatment temperatures, which indicates a lattice expansion.

The lattice parameters of α-Fe_2O_3 nanocrystals were calculated by a least-squares method using Retica Rietveld software. As illustrated in Figure 3a, with a size reduction, the lattice volume increased, which is in agreement with our TEM observations. Similar phenomena have also been observed in the literature for α-Fe_2O_3 microcrystals and ball-milled hematite nanocrystals.[13] On the other hand, we also found that the axial ratio of c/a became larger with a size reduction (Figure 3b), which is associated with an anisotropic expansion of the unit cell as

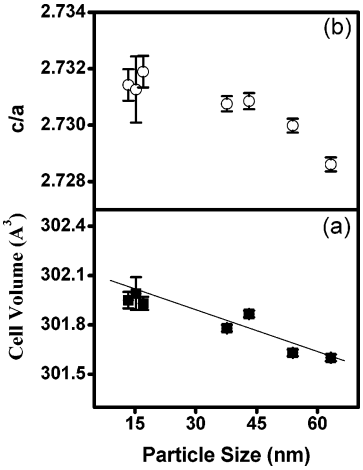

Figure 3. Size-induced variations of (a) cell volume *V* and (b) axial ratio, *c*/*a*.

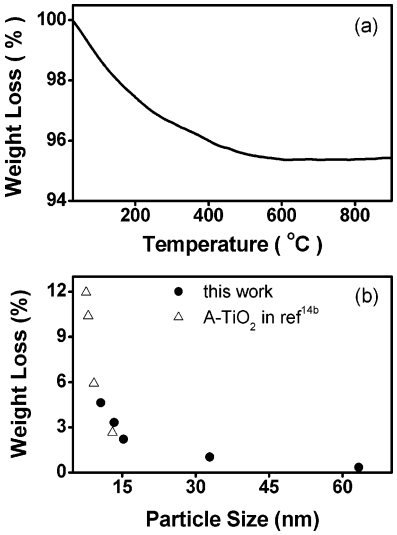

Figure 4. (a) TGA curve for 10 nm α-Fe_2O_3 (FE270) and (b) particle size dependence of weight loss for α-Fe_2O_3 nanocrystals as compared to that of anatase A-TiO_2 nanocrystals.[14b]

followed by a significant elongation of *c*-axis length relative to *a*-axis. The lowering symmetry of the structural units at small sizes is opposite to what was suggested by Ayyub et al.[9]

Nanocrystals, when exposed to aqueous environment, might have surfaces hydrated.[14] The hydration effects of α-Fe_2O_3 nanocrystals at different sizes are examined using TGA analysis. The TGA curve for 10 nm α-Fe_2O_3 (FE270) is shown in Figure 4a. It is seen that the mass loss occurs in a wide temperature range from room temperature up to 600 °C. Similar thermal behaviors were found for other sizes of α-Fe_2O_3. The relative mass in Figure 4a is almost an exponential decay from temperature lower than 100 °C to those above 400 °C. The distinct mass loss at temperatures lower than 100 °C indicates the presence of free water or physisobed water, while the continuous decay of relative mass versus temperature suggests that, for our α-Fe_2O_3 nanocrystals, the surface water molecules most likely exist in a wide set of energetically nonequivalent surface hydration groups. When the temperature is beyond 600 °C, the sample mass becomes constant. From the mass difference in TGA data indicated in Figure 4a, the total water content for 10 nm α-Fe_2O_3 was determined to be as high as 4.5 wt %. With increasing particle size, the total water content for the surface hydration sphere of α-Fe_2O_3 nanocrystals was decreased

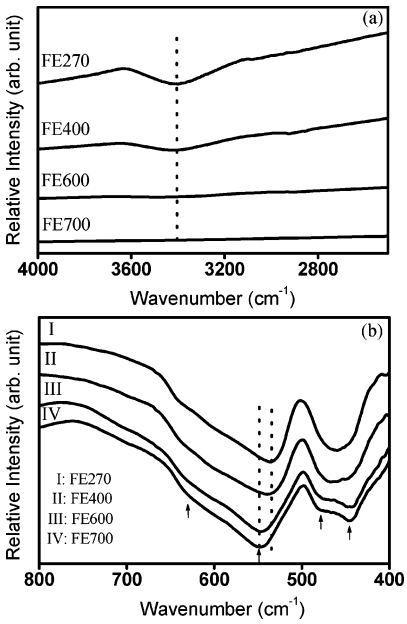

Figure 5. Infrared absorption spectra of α-Fe_2O_3 nanocrystals over wavelength ranges of (a) 2500−4000 and (b) 400−800 cm^{-1}.

monotonically (Figure 4b). This is the first report on the size dependence of the water content in α-Fe_2O_3 nanocrystals. From Figure 4b, it is also interesting that the water content for given sizes of α-Fe_2O_3 nanocrystals just falls onto the particle size dependence of water content as revealed recently by us for anatase TiO_2 nanocrystals.[14b]

The finite size effects on the vibrational properties of α-Fe_2O_3 nanocrystals were studied by infrared spectroscopy within a middle infrared range. As indicated in Figure 5a, a strong absorption band was observed at about 3500 cm^{-1} for sample FE270, which primarily originates from the surface hydration layers. With increasing treatment temperatures, the absorption bands associated with the hydration layers became weaker and absent in FE700. On the other hand, the broad absorptions observed in the range of 400−800 cm^{-1} (Figure 5b) were apparently composed of four vibrational modes centered at about 440, 480, 540, and 630 cm^{-1}. Group theoretical analysis predicts that α-Fe_2O_3 lattice has six infrared active modes,[15] among of which two infrared active modes are associated with the vibrations parallel to *c*-axis, while other four activate modes are those perpendicular to *c*-axis. Hayashi et al.,[16] calculated the infrared spectra of α-Fe_2O_3 and gave the assignments to these vibrations. According to the assignments in the literature,[11b,16] the absorptions observed at about 480 and 540 cm^{-1} in Figure 5b for our nano α-Fe_2O_3 can be ascribed to the perpendicular modes of the Fe−O stretching vibrations in corundum structure, while the absorptions at 630 and 440 cm^{-1} were associated with the modes that have polarization parallel to *c*-axis. From Figure 5b, it is noted that with lowering treatment temperature (also size reduction), the frequency of perpendicular mode at about 540 cm^{-1} showed a systematic red shift toward lower frequencies. Correspondingly, both vibration modes at 440 and 480 cm^{-1} merged into one narrow absorption, as is manifested by the arrows in Figure 5b.

The electronic transitions in α-Fe_2O_3 nanocrystals at different sizes were explored by measuring the visible and near-infrared diffuse reflectance spectra. Figure 6 shows a diffuse reflectance spectrum of FE700 in the visible region which is characterized by three prominent absorption bands near 865, 670, and 560 nm. These absorptions can be assigned[8] to the $^6A_1 \rightarrow {}^4T_1(^4G)$ and $^6A_1 \rightarrow {}^4T_2(^4G)$ ligand field transitions of Fe^{3+}, as well as

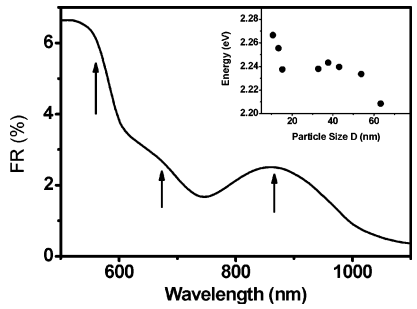

Figure 6. Diffuse reflectance spectrum of sample FE700. Inset shows the relationship between the transition energy of DEP and particle size.

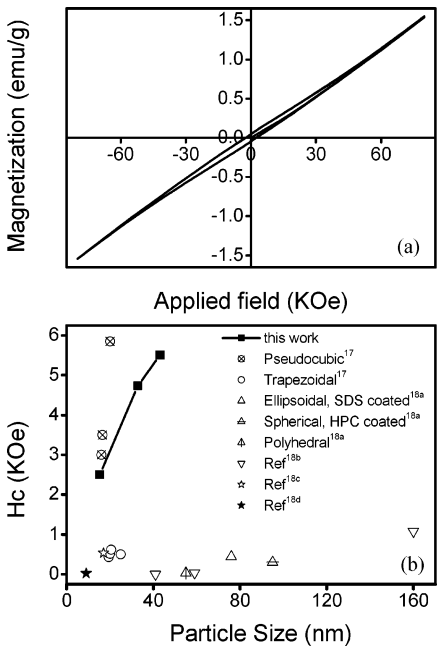

Figure 7. (a) Magnetization curve of FE400 and (b) coercive forces H_c's for samples at different sizes. Several reference H_c data were also given for comparison.

the $^6A_1 + {}^6A_1 \rightarrow {}^4T_1(^4G) + {}^4T_1(^4G)$ "double excition process" (DEP) of the simultaneous excitation of two adjacent Fe^{3+} centers (here $^6A_1$ and $^4T_1(^4G)$ represent the ground state and the first excited-state configurations of the high-spin Fe^{3+}, respectively). The electronic transition for DEP is much more intense comparing with other two transitions, here we use the transition of DEP to address size effects on the electronic levels of α-Fe_2O_3 nanocrystals. The inset of Figure 6 shows the transition energy of DEP as a function of particle size of α-Fe_2O_3 nanocrystals. From inset of Figure 6, it is seen that the transition energy of DEP exhibited a blue shift with a size reduction.

The magnetization curve of FE400 is shown in Figure 7a. Nearly identical magnetic hysteresis loops (except for the magnetic parameters) were also obtained for other sized samples. It is clear that α-Fe_2O_3 nanocrystals exhibited a weak ferromagnetic nature. The coercive forces, H_c's, for the samples are illustrated in Figure 7b, in which several reference H_c data were also given for comparison. H_c's of the present samples became larger with increasing particle size, which might be associated with the anisotropic energy barriers for rotation of magnetic moments that are proportional to the particle volume. It is interesting to note from Figure 7b that H_c's of our samples are much closer to the highest coercive forces already reported in the literature for highly agglomerated pseudocubic hematite nanoparticles.[17,18]

Discussion

α-Fe_2O_3 is analogous to many corundum-type oxides such as α-Al_2O_3 and α-Cr_2O_3 and serves as useful model systems for investigating oxide surface structure and reactivity. It is known that the surface hydration structures of nanoscale materials play significant roles in modifying the structural and electronic properties for reactivity improvements. Many theoretical and experimental investigations have been performed to study the hydration of corundum-type oxides and their surface energies.[19] Concerning the chemisorption of single-crystal Fe_2O_3,[20] the hydroxylation of the surfaces is reported to give lowered surface energy. Kurtz and Heinrich[21] have investigated the water adsorption on the basal plane of hematite, but they found that this surface was very inert and that exposure to very high amounts of water was necessary for creation of chemisorption. Apparently, all conflicting results relating to the surface hydration chemistry are owing to a lack of knowledge about finite size effects of surface hydroxylation. As Navrotsky had pointed out, the sizes and structures of nanoscale solids are highly correlated with the surface hydration, and dehydration and coarsening may occur simultaneously.[22]

With regards to the structural factors that are responsible for surface hydration, it is known that α-Fe_2O_3 crystallizes in a structure that consists of a distorted hexagonally closest packed layer sequence of oxygen with iron occupying two-thirds of the octahedral holes. The atomic layer stacking sequence along *c*-axis consists of six oxygen layers and 12 iron layers, which can be represented by the repeat of six stoichiometric -(Fe−O_3−Fe)- sequences per unit cell. Fe atoms are staggered along *c*-axis from their ideal position centered between the oxygen layers. As a consequence, the chemical clean termination of top three atomic layers for α-Fe_2O_3 (e.g., for (0001) surface)[23] can be described as a single iron-layer (Fe−O_3−Fe−R), a double iron-layer (Fe−Fe−O_3−R), or an oxygen-layer (O_3−Fe−Fe−R), where R represents the remaining atomic layers that keep the bulk unit cell stacking sequence. When in contact with moisture or being prepared from aqueous solutions, as predicted by a density functional theory calculation,[23] the clean surfaces would become hydroxylated mainly in the forms of termination configurations including $(HO)_3$−Fe−H_3O_3−R and $(HO)_3$−Fe−Fe−R that have significantly lower free energies than their dehydroxylated counterparts. Regardless the termination configurations, the outmost $(OH)_3$ species for the hydration sphere of α-Fe_2O_3 is most likely to be a function of the surface area (also the particle size). With the dehydration proceeding, the hydrated surface structure could be rearranged into a more stable configuration. This explained the continuous mass loss of α-Fe_2O_3 nanocrystals up to 600 °C (Figure 4a) and their significant size dependence, as is observed in Figure 4b.

To understand the correlation of surface hydration with the vibrational properties and bonding nature, it is necessary to examine the structural factors that may influence the frequencies of the absorption bands of α-Fe_2O_3. It is well-known that morphological variations, disorder−order transition, and surface effects can have impacts on the polarization fields at surfaces and hence the absorption peaks. Since all α-Fe_2O_3 nanocrystals reported in this work were prepared using the same methodology and the particle shapes are quite similar (see TEM photos for FE400 and FE600, top of Figure 2), the roles that the morphological variations played in the redshift observed in the vibration frequencies in Figure 5b could be ignored. It is noted that for α-Fe_2O_3 nanocrystals, the surface effects could become significant at small sizes due to a decrease in the symmetry of

surface atoms[24] or/and to a large amount of unsaturated surface states of Fe^{3+}.[25a] Although the nanoparticle surfaces stayed in air or prepared from aqueous solution would retain octahedral coordination with oxygen via the absorption of surface water molecules (Figures 4and 5a), the geometry of the coordination sphere at the surfaces of α-Fe_2O_3 nanocrystals would be slightly distorted by producing certain degree of long-range disorder within the few top surface layers.[24] Nevertheless, for α-Fe_2O_3 nanocrystals, as demonstrated by our TEM observations, the sample crystallinity is very high, while the surface structural disordering or amorphous phase is hard to see. Therefore, the large broadening of infrared bands from disordering was not observed in the absorptions within the wavelength range of 420−500 cm^{-1} (Figure 5b). Further, just like what happened in many other systems,[26] the lattice disordering can yield some new disorder-activated modes or the variations in the intensity, while the absorption positions remain unchanged. Therefore, the spectral red shift as illustrated in Figure 5b by the vibrational spectra of α-Fe_2O_3 at small sizes cannot be ascribed to the disorder−order transition of the lattice or the amorphous to crystalline phase transition.

What, then, is the nature for the significant red-shift of the absorption bands observed in Figure 5b? To answer this question, it is essential to differentiate the effects of lattice size and the particle size that might simultaneously contribute to the lattice vibrations of α-Fe_2O_3. Such a goal seems impossible to reach because the size reduction of α-Fe_2O_3 nanocrystals is closely related to a lattice expansion (Figure 3a). At a first approximation, we proposed that the particle size effects on lattice vibrations for nanocrystals are ignored when comparing to the particle size effects for the submicron counterparts. This is because for sufficiently large sizes (i.e., beyond submicron level for this work), the surface-to-volume ratio becomes extremely low, and the lattice dimensions would reach the equilibrium values that are supposed to be the same as those of the bulk. Wang et al.,[12] studied systematically the absorption frequencies of micron α-Fe_2O_3 at different equivalent diameters. However extrapolation of their diameter dependence of the absorption frequencies gives roughly constant absorption positions at nanoscale regime. Therefore, the red shift observed in the perpendicular mode at 540 cm^{-1} (Figure 5b) can be predominantly ascribed to the size-induced lattice variations. This reasoning is most likely the truth since, with a size reduction, the surface water content is largely increased by surface stabilization and reconstruction.[27a] The force constant of the interior lattice and the exchange-interactions among the particles[25b] can be hence tuned by finite size effects. For other iron oxide nanocrystals such as γ- Fe_2O_3 nanocrystals,[27a] the strains introduced during the formation of water monolayer on the nanoparticles surface have yielded certain variations in lattice parameters. But from the kinetic viewpoint, the strains are generally compressive. Consequently, the equilibrium lattice parameters were decreased, while the force constants between pairs of ions were increased for ionic bonding or covalent bonding. Lattice contraction has been reported for γ-Fe_2O_3 nanocrystals[27a] upon surface hydration because of the reduced surface dipole moments. Nevertheless, our recent work on rutile TiO_2 nanocrystals[27b] demonstrated that the strong repulsive forces among the roughly parallel surface defect dipoles from distorted structural unit polyhedra might give rise to a negative pressure by producing a lattice expansion. As such, for this work, the force constant between the pairs of $Fe^{3-}-O^{2-}$ for the intrinsic lattice vibrations could be smaller, since the corresponding lattice expansion in α-Fe_2O_3 nanocrystals became significant with a size reduction (Figure 3). The vibrational frequencies were thus decreased. This hypothesis is indicated by comparing the vibrational frequencies of corundum-type oxides α-Fe_2O_3 and α-Cr_2O_3 because for both compounds, the atomic weight is almost the same just like what our α-Fe_2O_3 nanoparticles have at different sizes, and because the difference in frequencies should solely originate from the difference in force constant. Indeed, Onari et al.,[22] observed that the infrared absorption frequencies for α-Fe_2O_3 are all smaller than those of α-Cr_2O_3, which is consistent with larger interionic distance of 2.09 Å between the oxygen and metal ion for α-Fe_2O_3 than that of 2.01 Å for α-Cr_2O_3.

The lattice modifications by surface hydration are also represented by an increase in axial ratio of *c*/*a* in Figure 3b. We believe a size reduction in α-Fe_2O_3 is equivalent to an application of a negative pressure, which is expected to get the lattice symmetry lowered owing to the anisotropic nature of α-Fe_2O_3 lattice. This elucidation is confirmed by a surface study[28] on 10 nm hematite nanocrystals where a decrease in symmetry had been demonstrated in the average coordination environment of surface atoms. Further, the axial ratio of *c*/*a* at small sizes should presumably vary in an opposite way from that of bulk α-Fe_2O_3 when compressed under high positive pressures. This has also been verified by a decrease in axial ratio of *c*/*a* in a high-pressure observation.[10] It is noted that the increases in axial ratio of *c*/*a* at small sizes indicated in Figure 3b strongly disprove the earlier conjectures[4,9] in which nanometer sized α-Fe_2O_3 phase is unstable below 30 nm and would transform into a structure of higher symmetry with a size reduction. These results are very important in dealing with the problems still remained about the distinct electronic (or magnetic) properties of α-Fe_2O_3 nanocrystals since the significant roles played by size-induced lattice modifications have been popularly ignored in the literature.

With regards to the finite size effects on the electronic transitions, it is essential to take into account the nature of Fe−O bonds of α-Fe_2O_3 at small sizes. As mentioned above, α-Fe_2O_3 shows a basic geometry consisting of hexagonal close-packed oxygen layers along *c*-axis with Fe occupying two-thirds of the octahedral sites and O being surrounded by four Fe ions. For high-spin Fe^{3+} ions of an octahedral symmetry, the energy of DEP transition is given approximately by[29]

$$E = -10Dq + 10B + 6C - \frac{26B^2}{10Dq} \quad (1)$$

$$\frac{Dq(P)}{Dq_0} = \left(\frac{V_0}{V(p)}\right)^{5/3} \quad (2)$$

where $10Dq$ denotes the crystal field splitting and B and C are Racah parameters that describe the neighboring covalency effect in transition metal systems.[29] Although there exist certain variations in $10Dq$ for different sizes of α-Fe_2O_3, the contribution of the term $10Dq$ to the relative transition energy (ΔE) might be very limited and could be neglected due to the small magnitude of lattice expansion in Figure 3b when considering the pressure dependence of Dq (equation 2). Second-order term ($-26B^2/10Dq$) is also extremely small in comparison with the sum of $10B$ and $6C$, as deduced using the estimated ligand field theory parameters in the literature.[8] Therefore, the blue shift observed in transition energy of DEP with a size reduction (inset of Figure 6) is most likely the consequence of an increase in Racah parameters (B and C). This is correct since, owing to the opposite pressure effects, the Racah parameters induced by size reduction will behave in a totally different way from that

of the bulk under high pressures.[29] In the latter cases, the Racah parameters are decreased with increasing external pressures. Even though the absolute values of Racah parameters of α-Fe_2O_3 nanocrystals are still hard to achieve at present, the size-induced increases in these parameters clearly demonstrated an ionicity enhancement. This enhancement can be rationalized by an increase in Fe−O separation during the anisotropic expansion at small sizes, since the lattice expansion may alter the distribution of crystal fields and charge cloud by depressing the electron affinity of Fe^{3+}. As a consequence, the results reported in this work might have broad implications in electronic transition that could be tailored by finite size effects and bonding modifications.

The electronic structures and fundamental bonding properties of the $Fe^{3+}-O^{2-}$ also determine the magnetic anisotropy coefficients and hence the magnetic behaviors.[18b,30] Generally, the coercive forces are predominantly determined by surface and finite-size effects. The surface effects that are highly hydrated become more and more important as the particle size decreases due to the increase of surface-to-volume ratio and the weakened exchange coupling that originated from the breaking of lattice symmetry and unsaturated bonds. Although the hydration molecules, as mentioned above, could be bonded to the surface by lowering the surface energy, the surface spins are mostly likely to deviate from the anti-ferromagnetic alignment, which allows a variety of reversal upon cycling the applied field and results in the large coercivities that are apparently opposite to what we have observed in Figure 7. Indeed, for the interior lattice of the nanoparticles when assuming as the single domains, the coercive force can be described below according to the Bean−Livingston equation:[31]

$$H_c = \frac{2KV}{\mu}[1 - (T/T_b)^{1/2}] \quad (3)$$

where K is the magnetocrystalline anisotropy, V is the particle volume, μ is the magnetic moment of the particle, and T_b is the blocking temperature above which the particle is superparamagnetic in zero magnetic field. From equation 3, it is clear that H_c decreases with a size reduction (also particle volume V). Just as in other magnetic nanoparticles,[32] with a size reduction, the fraction of the surface region of hydration increases, which may give rise to a smaller magnetocrystalline anisotropy. The balance between the finite and surface effects could explain the decrease of coercive force with a size reduction in α-Fe_2O_3 nanoparticles. It should be mentioned that the surface hydration also influences the magnetic behavior of our α-Fe_2O_3 nanoparticles or even other magnetic nanoparticles by reducing the interparticle magnetic interactions[25b] and the energy barriers for magnetic anisotropy. Besides all of these, as illustrated in Figure 2, our samples have much higher crystallinity, which accounts for the considerably large H_c's.

In summary, this work reports the finite size effects on the structural relevant electronic transitions in α-Fe_2O_3 nanocrystals. It is found that α-Fe_2O_3 nanocrystals exhibited highly hydrated surfaces that are strongly particle size dependent. With size reduction, the lattice volume increased, which was accompanied by an enlarged axial ratio and a large lattice distortion, in apparent contradiction to the previous literature work that nanometer sized α-Fe_2O_3 is becoming to a structure of higher symmetry. The finite size effects in α-Fe_2O_3 nanocrystals were demonstrated by a red shift in vibrational frequencies of perpendicular mode at 540 cm^{-1}, a blue shift in the electronic transition for double exciton process in visible region, and a striking decrease in coercive force.

Acknowledgment. This work was supported by a grant of Hundred Talents Plan of China (Li G) and a grant under the contract (No. 2004HZ01-1) from Fujian Province, P. R. China.

References and Notes

(1) Fiorani, D.; Testa, A. M.; Suber, L.; Angiolini, M.; Montone, A.; Polichetti, M. *Nanostruct. Mater.* **1999**, *12*, 939.

(2) Muench, G. J.; Srajs, S.; Matljevic, E. *Phys. Stat. Sol. A* **1985**, *92*, 187.

(3) (a) Zhang, J. Z. *J. Phys. Chem. B* **2000**, *104*, 7239. (b) Toledano, D. S.; Henrich, V. E. *J. Phys. Chem. B* **2001**, *105*, 3872. (c) Waite, T. D. Ph D. Dissertation, Massachusetts Institute of Technology, Cambridge, MA, 1983.

(4) Ayyub, P.; Multani, M.; Barma, M.; Palkar, V. R.; Vijayaraghavan, R. *J. Phys. C* **1988**, *21*, 2229.

(5) Madden, A. S.; Hochella, M. F. *Geochim. Cosmochim. Acta* **2005**, *69*, 389.

(6) Katsuki, H.; Shiraishi, A.; Komarneni, S.; Moon, W. J.; Toh, S.; Kaneko, K. *J. Ceram. Soc. Jpn.* **2004**, *112*, 384.

(7) Yi, J. H.; Son, S.; Choi, M. *Key Eng. Mater.* **2002**, *206*, 135.

(8) Sherman, D. M.; Waite, T. D. *Am. Mineral.* **1985**, *70*, 1262.

(9) Ayyub, P.; Palkar, V. R.; Chattopadhyay, S.; Multani, M. *Phys. Rev. B* **1995**, *51*, 6135.

(10) Liu, H.; Caldwell, W. A.; Benedetti, L. R.; Panero, W.; Jeanloz, R. *Phys. Chem. Miner.* **2003**, *30*, 582.

(11) (a) Serna, C. J.; Ocana, M.; Iglesias, J. E. *J. Phys. C* **1987**, *20*, 473. (b) Serna, C. J.; Rendon, J. L.; Iglesias, J. E. *Spectrochimica Acta A* **1982**, *38*, 797.

(12) Wang, Y. S.; Muramatsu, A.; Sugimoto, T. *Colloids Surf. A* **1998**, *134*, 281.

(13) (a) Schroeer, D.; Nininger, R. C. *Phys. Rev. Lett.* **1967**, *19*, 632. (b) Stewarta, S. J.; Borzi, R. A.; Cabanillas, E. D.; Punte, G.; Mercader, R. C. *J. Magn. Magn. Mater.* **2033**, *260*, 447.

(14) (a) Navrotsky, A. *Geochem. Trans.* **2003**, *4*, 34. (b) Li, G. S.; Li, L. P.; Boerio-Goates, J.; Woodfield, B. F. *J. Am. Chem. Soc.* **2005**, *127*, 8659. (c) Linsebigler, A. L.; Lu, G. Q.; Yates, J. T. *Chem. Rev.* **1995**, *95*, 735.

(15) Onari, S.; Arai, T.; Kudo, K. *Phys. Rev. B* **1977**, *16*, 1717.

(16) Hayashi, S.; Kanamori, H. *J. Phys. C* **1980**, *13*, 1529.

(17) (a) Rath, C.; Sahu, K. K.; Kulkarni, S. D.; Anand, S.; Date, S. K.; Das, R. P.; Mishra, N. C. *Appl. Phys. Lett.* **1999**, *75*, 4171.

(18) (a) Jing, Z. H.; Wu, S. H.; Zhang, S. M.; Huang, W. P. *Mater. Res. Bull.* **2004**, *39*, 2057. (b) Raming, T. P.; Winnubst, A. J. A.; Kats, C. M. V.; Philipse, A. P. *J. Colloid Interface Sci.* **2002**, *249*, 346. (c) Li, G. S.; Smith, J. R.; Inomata, H.; Arai, K. *Mater. Res. Bull.* **2002**, *37*, 949. (d) Deb, P.; Basumallick, A.; Chatterjee, P.; Sengupta, S. P. *Scripta Mater.* **2002**, *45*, 341.

(19) (a) McHale, J. M.; Navrotsky, A.; Perrotta, A. J. *J. Phys. Chem. B* **1997**, *101*, 603. (b) Jones, F.; Rohl, A. L.; Farrow, J. B.; Bronswijk, W. V. *Phys. Chem. Chem. Phys.* **2000**, *2*, 3209. (c) Kittaka, S.; Umezu, T.; Ogawa, H.; Maegawa, H.; Takenaka, T. *Langmuir* **1998**, *14*, 832.

(20) (a) Liu, P.; Kendelewicz, T.; Brown, G.; Nelson, E.; Chambers, S. *Surf. Sci.* **1998**, *417*, 53. (b) Herman, G.; McDaniel, E.; Joyce, S. *J. Electron Spectrosc. Relat. Phenom.* **1999**, *101*−*103*, 433.

(21) Kurtz, R. L.; Heinrich, V. E. *Phys. Rev. B* **1983**, *36*, 3413.

(22) Navrotsky, A. *Proc. Natl. Acad. Sci. U.S.A.* **2004**, *101*, 12096.

(23) Trainor, T. P.; Chaka, A. M.; Eng, P. J.; Newville, M.; Waychunas, G. A.; Catalano, J. G.; Brown, G. E. *Surf. Sci.* **2004**, *573*, 204.

(24) Zhang, J.; Wu, Z. Y.; Ibrahim, K.; Abbas, M. I.; Ju, X. *Nucl. Instrum. Methods Phys. Res. B* **2003**, *199*, 291.

(25) (a) Chen, L. X.; Liu, T.; Thurnauer, M. C.; Csencsits, R.; Rajh, T. *J. Phys. Chem. B* **2002**, *106*, 8539. (b) Predoi, D.; Kuncser, V.; Tronc, E.; Nogues, M.; Russo, U.; Principi, G.; Filoti, G. *J. Phys. C* **2003**, *15*, 1797.

(26) (a) Ingale, A.; Rustagi, K. C. *Phys. Rev. B* **1998**, *58*, 7197. (b) Fahim, M. A. *Thermochimica Acta* **2000**, *363*, 121.

(27) (a) Belin, T.; Millot, N.; Villieras, F.; Bertrand, O.; Bellat, J. P. *J. Phys. Chem.* B. **2004**, *108*, 5333. (b) Li, G. S.; Boerio-Goates, J.; Woodfield, B. F.; Li, L. P. *Appl. Phys. Lett.* **2004**, *85*, 2059.

(28) Zhang, J.; Wu, Z. Y.; Ibrahim, K.; Abbas, M. I.; Ju, X. *Nucl. Inst. Methods B* **2003**, *199*, 291.

(29) Bray, K. L. *Top. Curr. Chem.* **2001**, *213*, 1.

(30) Lenglet, M.; Hochu, F.; Simsa, Z. *Mater. Res. Bull.* **1998**, *33*, 1821.

(31) Muench, G. J.; Arajs, S.; Matijevic, E. *J. Appl. Phys.* **1981**, *52*, 2493.

(32) (a) Xiao, Q. F.; Bruck, E.; Zhang, Z. D.; de Boer, F. R.; Buschow, K. H. J. *J. Alloys Compd.* **2004**, *364*, 64. (b) Koyama, T.; Onodera, H. *J. Jpn. Inst. Metals* **2004**, *68*, 1008.